Animation of computer simulations of two-dimensional turbulence and three-dimensional flows

by M. Briscolini
P. Santangelo

One of the most challenging problems in fluid dynamics is understanding the properties of turbulent flows. The advent of large supercomputers permits the investigation of turbulence with great accuracy in two dimensions, but full three-dimensional problems are physically more complex and their study is currently limited to the case of simple flows. It is shown that the availability of a continuous time-dependent representation of the dynamics of fluid flows can quickly lead to more complete understanding of the many concurrent physical mechanisms ruling turbulence. Some significant examples show how an analog videotape, obtained from direct computer simulations of fluid flows, suggests physical results that can later be obtained through a mathematical analysis of the numerical simulations.

Introduction

The word *turbulence* generally indicates the chaotic behavior of a fluid. Far from being an exceptional phenomenon, turbulent flows rule the behavior of many fluids occurring in nature. It can easily be observed that fluids frequently tend to behave chaotically rather than regularly; the air flowing around a moving car and that moving past a flying airplane are two examples of very turbulent flows. It is worthwhile to note that many phenomena occurring in geophysics, astrophysics, and plasma physics are completely dominated by more or less turbulent flows. An example is given by the motion of the atmosphere, which is very turbulent over scales ranging from many thousands of kilometers down to millimeters. Consequently, the problems connected to weather forecasts are among the most important unresolved issues from both the scientific and the computing points of view. Indeed, given a hypothetical,

infinitely powerful computer, one of the open questions in meteorology is the feasibility of reliable and long-time-range weather forecasts.

The equation of motion of a fluid is the well-known Navier–Stokes equation, first written approximately a century ago. This equation derives from the principle of conservation of momentum and includes the viscous terms describing the conversion of mechanical energy into heat. In the general case, this equation is

$$\frac{\partial \bar{u}}{\partial t} + (\bar{u} \cdot \bar{\nabla})\bar{u} = -\frac{\bar{\nabla} p}{\rho} + \eta \Delta \bar{u} + \left(\zeta + \frac{\eta}{3}\right)\bar{\nabla}(\bar{\nabla} \cdot \bar{u}) + \text{forcing}, \quad (1)$$

where $\bar{u}$ is the velocity field, p is the pressure, ρ is the density, η and ζ are the viscosity coefficients, and the differential operators are defined according to standard notation [1]. In addition to Equation (1), the mass-conservation equation and an energy-transfer equation are required in order to have a complete system of partial differential equations with five scalar equations for the five unknown fluid dynamic fields $\bar{u}$, p, and ρ.

Although (1) is the equation to be used in the general case, in the following we concentrate on the simple case for which the density ρ is constant, so that only one equation in addition to Equation (1) is needed to complete the system. The required equation is the one for conservation of mass, which here simply reduces to $\bar{\nabla} \cdot \bar{u} = 0$ so that no energy-transfer equation is needed. Consequently, (1) simplifies to

$$\frac{\partial \bar{u}}{\partial t} + (\bar{u} \cdot \bar{\nabla})\bar{u} = -\frac{\bar{\nabla} p}{\rho} + \nu \Delta \bar{u} + \text{forcing}, \quad (2)$$

where $\nu = \eta/\rho$ is the kinematic viscosity (hereafter referred to simply as viscosity). A further simplification can be obtained by substituting the vector identity

$$(\bar{u} \cdot \bar{\nabla})\bar{u} = \frac{1}{2}\bar{\nabla} u^2 - \bar{u} \times (\bar{\nabla} \times \bar{u}) \quad (3)$$

in (2) and taking the curl of the equation:

$$\frac{\partial \bar{\omega}}{\partial t} + (\bar{u} \cdot \bar{\nabla})\bar{\omega} = (\bar{\omega} \cdot \bar{\nabla})\bar{u} + \nu \Delta \bar{\omega} + \text{forcing}, \quad (4)$$

where $\bar{\omega} = \text{curl}\ \bar{u} = \bar{\nabla} \times \bar{u}$ is the vorticity vector. Equation (4) turns out to be particularly useful because it contains only kinetic fields; moreover, the nonlinear term has been usefully split into two parts: The left-hand side describes the advection of vorticity due to the velocity field, while the right-hand side describes the well-known phenomenon of *vortex stretching* [2], typical of the three-dimensional case and not occurring in two dimensions, as we shall see in Section 2.

In spite of their apparent simplicity, the nonlinear terms contained in the equations of motion of a fluid are a very challenging issue for both mathematicians and physicists. Despite all the above simplifications, analytical solutions of these equations are known only when the flow is regular (i.e., when the velocities do not vary rapidly inside the flow domain) and for very simple boundary conditions: These solutions always represent a fluid smoothly flowing around obstacles or inside a container. When the velocity field is no longer smooth, the fluid may begin to flow in a very complex and often unpredictable way, depending on the time and length scales of interest. There are many ways this can happen, but the investigation of this important and complex phenomenon, called *transition to turbulence* (see, e.g., [3]), is beyond the scope of this paper and is not analyzed further.

Well beyond the point where transition to turbulence takes place, one observes extremely rapid flow variations in both space and time: This kind of flow is called *developed turbulence*. The generally accepted belief is that, in the limit of very highly turbulent flows, the behavior of the fluid is ruled by general statistical laws whose investigation and comprehension is a very important fluid dynamics problem. Any attempt to derive such laws must take into account some statistical description of the problem as A. N. Kolmogorov did in the first successful and, so far, substantially unsurpassed work on three-dimensional turbulence [4].

The basic assumption of Kolmogorov's theory is that, in a turbulent flow, there is an approximate equilibrium of energy transfer from large to small scales. More precisely, this statistical theory states that energy is injected on a large scale by some external force, and is transferred through nonlinear instabilities to smaller and smaller scales in a continuous fashion until a minimum scale (the *dissipation scale*) is reached, where the flow becomes smooth and viscosity converts the kinetic energy into thermal energy. In particular, the theory assumes that the nonlinear term is active on all scales except the smallest ones and is responsible for the transfer (or *cascade*) of energy from large to small scales, while the dissipative operator $\nu\Delta$ is always negligible except on the smallest scales, where it dominates. Among the most successful results of the theory are the semi-quantitative estimates of the energy spectrum $E(k) \sim k^{-5/3}$ and of other measurable quantities, as a function of the Reynolds number and energy injection scale only.[1] These theoretical results are in good agreement with experimental data for the three-dimensional case, while in the simpler two-dimensional case new phenomena

[1] The Reynolds number is the nondimensional quantity defining an incompressible flow $Re = LU/\nu$, where L, U are respectively the characteristic length and the characteristic velocity of the problem.

tend to appear in the flow, as we shall see in the next section.

In the course of time many authors have attempted to refine Kolmogorov's description by adding new physics to the original theory (e.g., multifractals, as in [5] and references therein). Although these new features do not substantially change the original Kolmogorov scenario, they refine remarkably the agreement with experimental data in three dimensions [6].

In Section 2 we present some relevant results obtained from a pair of high-resolution numerical simulations of two-dimensional turbulence, for the first time with the aid of an analog videotape recording; the same tool is used in Section 3 to show how animation can enrich present-day comprehension of simple three-dimensional flows. Section 4 describes the details of the techniques used to produce the visualization of our computations.

2. Two-dimensional decaying turbulence

It might seem that any study of two-dimensional flow would be of academic interest only, since in nature all fluids are fully three-dimensional. On the contrary, many flows show properties that can be well approximated by a two-dimensional approach. Among these we find the remarkable example of the earth's atmosphere when this is studied over a large range of scales, from the planetary scale down to scales of a few hundred kilometers; another interesting example is the flow of fusion plasmas in Tokamak machines, whose two-dimensional nonlinear behavior has been successfully simulated in recent numerical experiments [7].

In two dimensions, the equation of motion (2) holds unchanged, while Equation (4) is substantially simplified because the vorticity vector $\bar{\omega}$ is always perpendicular to the flow plane and can be described by a simple scalar ω:

$$\frac{\partial \omega}{\partial t} + (\bar{u} \cdot \bar{\nabla})\omega = \nu \Delta \omega + \text{forcing}. \tag{5}$$

One sees that the main physical content of this equation is the advection of vorticity by the velocity field; it follows that, in a nonviscous and nonforced flow, vorticity is conserved along streamlines. We note incidentally that these equations do not contain the nonlinear vortex-stretching term contained in the right-hand term of Equation (4). A further simplification of Equation (5) comes from the definition of the stream function ψ as

$$u_x = -\frac{\partial \psi}{\partial y}, \qquad u_y = \frac{\partial \psi}{\partial x}, \tag{6}$$

which automatically satisfies the incompressibility condition ($\bar{\nabla} \cdot \bar{u} = 0$); vorticity is simply obtained as $\omega = \Delta\psi$. The general equation in two dimensions is thus

$$\frac{\partial \Delta \psi}{\partial t} + J(\psi, \Delta\psi) = \nu_p \Delta^{p+1} \psi + \text{forcing}, \tag{7}$$

where $J(a, b) = \partial_x a \partial_y b - \partial_y a \partial_x b$ is the Jacobian. Here we have introduced a useful generalization of the dissipative term, called *superviscosity*, that reduces to the standard one for $p = 1$ (see, e.g., [8]). One may wonder whether this apparent and somewhat arbitrary change in the structure of the equations is likely to have an important influence in any study of two-dimensional developed turbulence. The generally accepted answer is negative and is based on the fact that all statistical theories confine the rule of the dissipative term to the smallest scales, where dissipation really takes place (see, e.g., [8–10]). In other words, by increasing p, one can only change some details of the energy flow near the smallest scales without altering significantly most of the remaining large scales. Moreover, there is no laboratory measure of the functional form of dissipation for large Reynolds numbers, and the use of the classical (or molecular, $p = 1$) form of dissipation for developed turbulence is justified by no argument other than a strictly conservative approach. On the other hand, the use of superviscosity is of great importance in numerical simulations, where one always has a limited number of degrees of freedom; indeed, as a consequence of the form of the differential operator, by increasing p one makes more room for scales where the important and more interesting nonlinear phenomena take place (see [11], where $p = 8$ has usefully minimized the range of scales for which dissipation occurs).

In two dimensions, Kolmogorov's theory cannot be applied straightforwardly. The energy is prevented from being dissipated because of a well-known theorem that guarantees the small-scale regularity of the solution of the flow equations for any value of the viscosity coefficient ν_p. This phenomenon is the basis for the proper reformulation of Kolmogorov's description in two dimensions; this was done by Kraichnan [12] and Batchelor [13] in another theory hereafter referred to as KB. In this theory it is assumed that the energy associated with a flow domain with area A,

$$E = \frac{1}{2A} \int u^2 \, dV, \tag{8}$$

is substantially conserved and does not flow to small scales because of the previous regularity theorem; the role originally played by energy in the three-dimensional Kolmogorov theory is here played by a new quantity, the enstrophy, defined as

$$\Omega = \frac{1}{2A} \int \omega^2 \, dxdy. \tag{9}$$

The enstrophy is an interesting integral quantity that

indicates the amount of *rotational activity* inside the flow; in fact, the enstrophy density $1/2\omega^2$ is an important local quantity that measures directly the local fluid spinning velocity. The KB theory describes the equilibrium state of a two-dimensional turbulent flow as a continuous mechanism where enstrophy is injected at large scales, then flows nonlinearly toward small scales and eventually dissipates; this scenario turns out to be very similar to the standard Kolmogorov theory except that enstrophy now plays the role originally played by energy in three dimensions. In analogy with Kolmogorov's theory, the KB theory predicts the energy spectrum that corresponds to the enstrophy cascade: $E(k) \sim k^{-3} (\log k)^{-1/3}$; this is approximately

$$E(k) \sim k^{-3}. \tag{10}$$

The theory also allows for an inverse energy cascade, where the injected energy is transported to large scales, as has been verified by numerical experiments.[2]

The possibility of testing the KB theory has intrigued scientists for years, from the experimental as well as the numerical point of view (see, e.g., [8–11, 14, 15]. Since present-day supercomputers can treat two-dimensional flows with great accuracy (up to 1024×1024 in [10]), we present some physical results obtained from two numerical experiments of decaying turbulence, with the remarkable help of a color videotape animation.

Although no forced experiments are presented (these can be found elsewhere [11]), we think that this limitation is not severe, since decaying experiments do show some of the peculiar features of two-dimensional turbulence that make it so different from three-dimensional turbulence. All our experiments aim at comprehension of the dynamics of turbulence, and we have confined the flow domain to a simple, doubly periodic square with side 2π and a numerical resolution of 512×512. All the experiments use the pseudospectral technique to fully exploit the available degrees of freedom [16]. The field is evolved in time using the so-called wave-space, and the nonlinear terms are computed using fast Fourier transforms (FFTs). In principle, this method may show the well-known aliasing errors, although these errors are not expected to have a significant influence on any flows with a steep spectrum. However, severe aliasing errors appear when the spectrum flattens, as is observed in many simulations; for this reason, in all our simulations we make use of well-known de-aliasing procedures [17]. Time marching is performed by using a leapfrog scheme, combined with a Euler predictor-corrector scheme at regular intervals. All computations were performed using double precision, but we have observed that single precision can safely be used during the late stages of the numerical experiments to speed up the computation.

The numerical parameters of the models are initial energy $E = 0.5$, superviscosity with $p = 2$, and $\nu_2 = 2 \times 10^{-9}$. Wave numbers are normalized according to $K_J = 2\pi/\lambda_J$, $J = 0, 1, 2, \cdots, 512$. The time step is $\Delta t = 6.25 \times 10^{-4}$, and a total of 64 000 time steps have been performed to reach time $T = 40$. The computer code comprises only two-dimensional FFTs [18] and double DO-loops, so that the entire code can easily be vectorized over inner loops and parallelized over outer loops. The computations were performed on an IBM 3090[3]/600 Vector Multiprocessor using both MTF (MultiTasking Facility [19]) under MVS/XA[3] and PF (Parallel FORTRAN [20]) under MVS/XA or VM/XA[3]-SP2. The video recording equipment used an IBM AT[3] Personal Computer as a VM/CMS terminal to run the numerical experiment and simultaneously download each image onto a random-access laser videodisk recorder; no intermediate storage of images was used, because this would have required a prohibitive amount of mass storage (see Section 4 for a detailed description of the visualization techniques used.

• *An experiment with a self-similar spectrum*

In this first simulation we start from the spectrum

$$E(k) \sim k[1 + (k/k_0)^{\gamma+1}]^{-1}, \tag{11}$$

where k_0 is a reference wavelength. This is approximately a KB spectrum $E(k) \sim k^{-3}$ for our choice of $\gamma = 3$ and $k_0 = 6$; wave components with a given wavelength are generated as complex numbers with random phases and modulus obtained from a Gaussian random generator having zero mean and variance obtained from (11). As already indicated, superviscosity is used, with $p = 2$ and $\nu_2 = 2 \times 10^{-9}$. Similar experiments have been reported in [9, 15, 21].

Figures 1(a)–(f) show the most significant vorticity frames of the numerical evolution, and the corresponding videotape animation clearly indicates the many concurrent physical mechanisms that take place. In particular, one observes that the initial randomness is rapidly lost, probably due to the observed intense enstrophy dissipation of the initial phase. Concurrently, some of the initial small-scale vorticity peaks organize themselves into more and more regular structures that interact strongly [Figure 1(b), $t = 5$]. With time, the size of the structures tends to increase, due to an amalgamation process, up to a point where more or less

[2] R. Benzi, B. Legras, and P. Santangelo, IBM ECSEC, Rome, private communication.

[3] 3090, MVS/XA, and VM/XA are trademarks, and AT is a registered trademark, of International Business Machines Corporation.

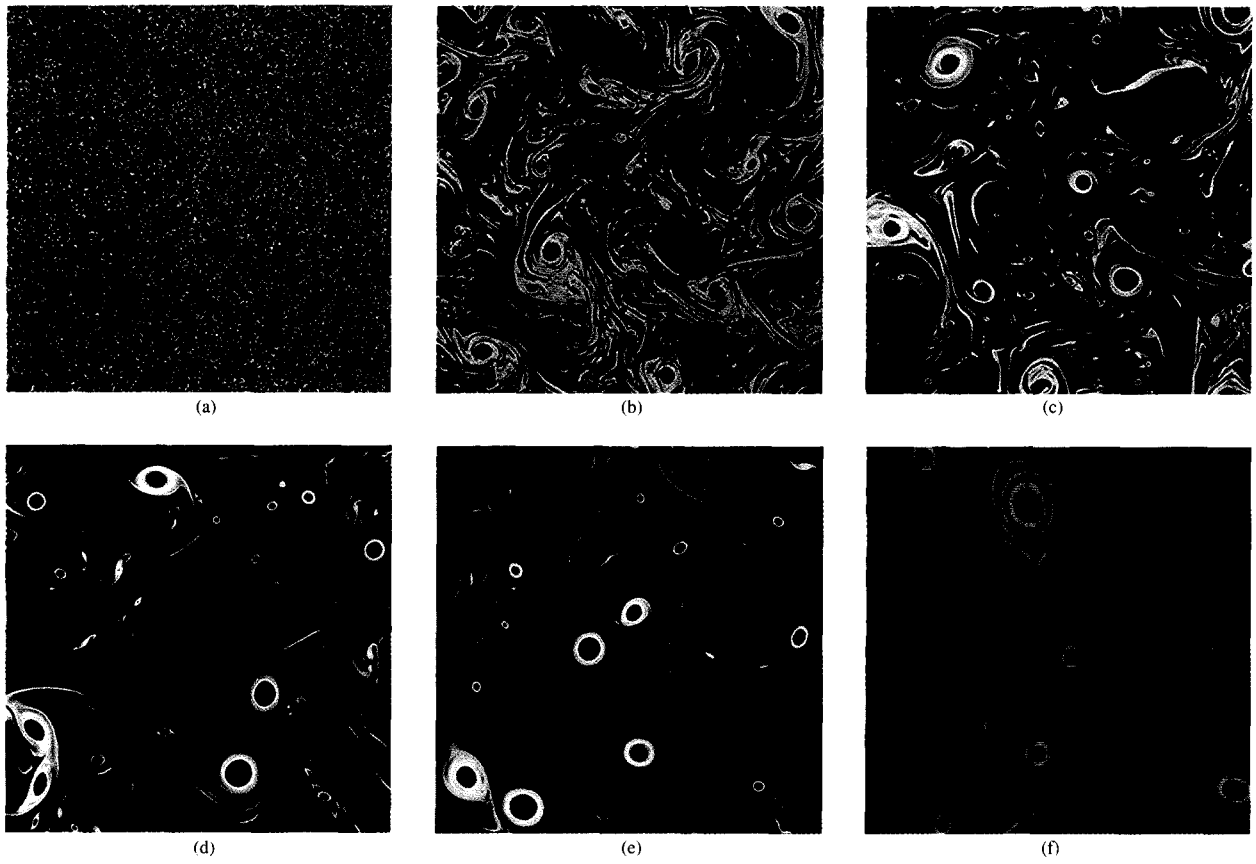

Figure 1

Decaying turbulence simulation of a Kraichnan–Batchelor initial spectrum. Instantaneous vorticity fields at times $t = 0$ (a), $t = 5$ (b), $t = 10$ (c), $t = 20$ (d), $t = 30$ (e), and $t = 40$ (f). Blue and red indicate clockwise and counterclockwise rotation, respectively. The color table is designed to enhance low-vorticity features significantly, as discussed in detail in Section 4; the maximum absolute value of vorticity is $|\omega| \sim 20$. Starting from highly random initial conditions, the system forms vortices whose size increases with time. The entire evolution shows several vortex collisions that usually lead to the merging of the two vortices if the encounter is close enough and the vortices have the same sign. The simulation is performed using a de-aliased pseudospectral technique on a 512×512 grid of collocation points; supervisscosity is used, with $p = 2$ and $\nu_2 = 2 \times 10^{-9}$ as in Equation (7).

isolated structures, hereafter named vortices, appear increasingly well separated from the rest of the fluid, which is more chaotic and of low absolute vorticity [Figures 1(b) and 1(c), $t = 5$ and 10]. The process that most evidently leads to the increase in vortex size is merging; this occurs when two vortices having the same sign approach each other closely enough to eventually combine into a single vortex. This phenomenon, shown in detail in **Figure 2** for a large vortex, has been studied theoretically in [22] (and references therein) and appears to be a nearly nondissipative process. More generally, these vortices appear to behave like a set of charged particles, as in electrostatics, but with an opposite interaction sign; vortices with the same sign attract each other, and eventually merge if they collide. In the case of collision of vortices with different signs, a temporary dipolar structure (see **Figure 3**), well-known as a *modon* (see, e.g., [2] and [23]), may form; its lifetime is generally short due to the strong disrupting interference of the rest of the vortices.

The phenomenon of merging is dominant during the first stages of this decaying-turbulence experiment. With time, one sees that larger and larger vortices form by merging, at the expense of smaller ones [Figures 1(c)–(f)], while a large fraction of small-scale vortices survives because of the increase in interparticle distance and the corresponding increase in collision mean free time. The final phases of the simulation are characterized by a hierarchy of vortices: the smaller the vortex size, the larger the corresponding number of vortices [see Figures 1(e) and 1(f)]. We note that all vortices have roughly the same maximum vorticity (same color intensity) in spite

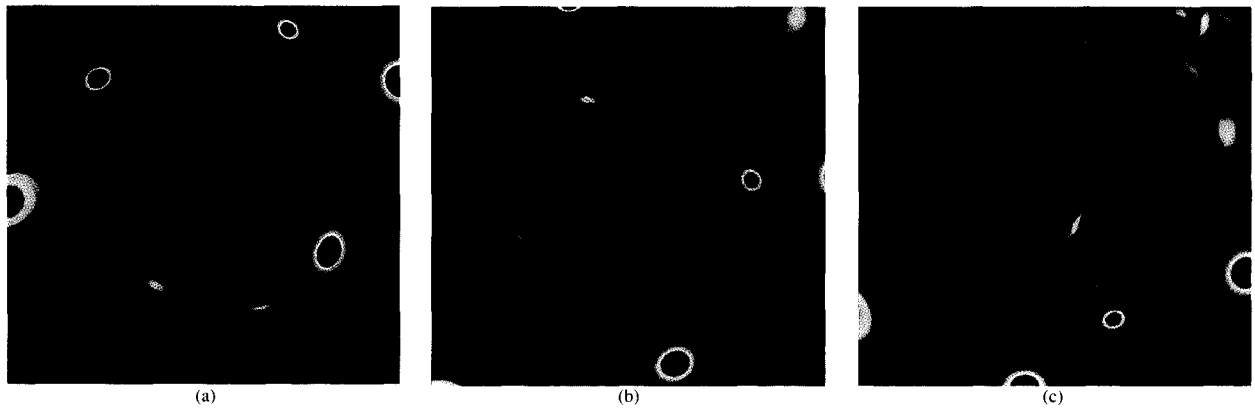

(a) (b) (c)

Figure 2

Detailed description of a merging event. Enlargement of Figure 1(e) showing a pair of blue (clockwise) rotating vortices, immediately after the beginning of the collision. In (a) (t = 30) the vortices rotate in a low-vorticity background having a rough spiral pattern, and the circular shape of the vortices already appears elongated because of their mutual interaction. In (b) (t = 31) the vortices are close to merging. In (c) (t = 32) merging has already occurred, and the newly formed vortex spins rapidly in an extended background; this is partly formed by the debris of the merging process and is dominated by filamentary components which will dissipate in a few time units (see Figure 7).

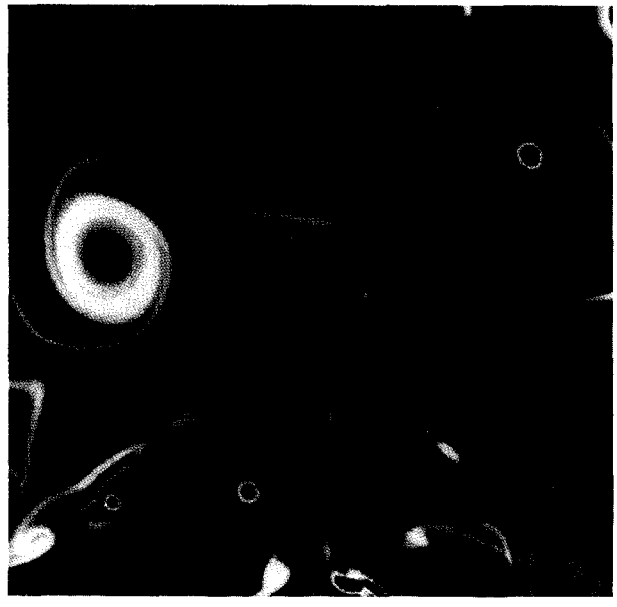

Figure 3

Temporary modon. Around time t = 16, a close collision of two vortices having different signs gives rise to the formation of a dipolar structure, or *modon* (see, e.g., [2] and [8]). Isolated modons may be shown to be stable, but their survival in a complex environment is closely related to the disrupting influence of the rest of the field. The enlargement shows a somewhat asymmetric and distorted modon which will decouple in few time units. Among the many temporary modons which are formed during the simulation, some may survive for many time units, as is shown in Figure 4.

of their very different sizes; in other words, all vortices rotate with nearly the same angular velocity.

During the last phases of the experiment, one sees that the fluid can be described more and more accurately as a pair of different systems. The first comprises only the vortices and appears to behave rather regularly; the second, comprising the rest of the fluid, shows a much more chaotic behavior and can be effectively imagined as a separated fluid driven by the same vortices. We discuss later some other results connected to this clear decoupling of the flow.

Since the number of merging events tends to decrease at the end of the simulation, it is interesting to undertake a careful study of the trajectories of the isolated vortices. **Figure 4** indicates how, during this *quiet* phase, all vortices move rather smoothly over very long time scales (comparable to a *crossing time*, i.e., the time that a vortex takes to cross the flow domain). It is also interesting to simulate these trajectories with an inviscid Hamiltonian describing a few interacting point vortices to find a remarkable correspondence of the trajectories (see [15] for details of such a comparison).

The phenomenon of the smoothness of vortex trajectories, shown in Figure 4, is a remarkable one because it shows how the most important degrees of freedom of this turbulent flow, namely the vortices, have a rather *predictable* motion over time scales of many units. This result is strengthened by comparison with the time scales connected to the background fluid component. These turn out to be much smaller, by more

than an order of magnitude, as is shown in the more detailed analysis found in [15]. This statement is further strengthened by comparison with another small time scale, the vortex *spinning time*: $T_{spin} = 2\pi/\omega_{max} \sim 0.15$.

An important result concerning the dynamics regards the time evolution of the energy spectra. This shows that the initial spectrum $E(k) \sim k^{-3}$ is not stationary, but soon changes toward spectra which still retain a similar shape but show a much larger steepness (**Figure 5**). Whether or not these decaying (and not forced) experiments can be fully compared with the KB scenario is an open question that requires more numerical resolution and computing power. A preliminary indication can be found in [11], where all high-resolution forced experiments show spectra significantly steeper than k^{-3}.

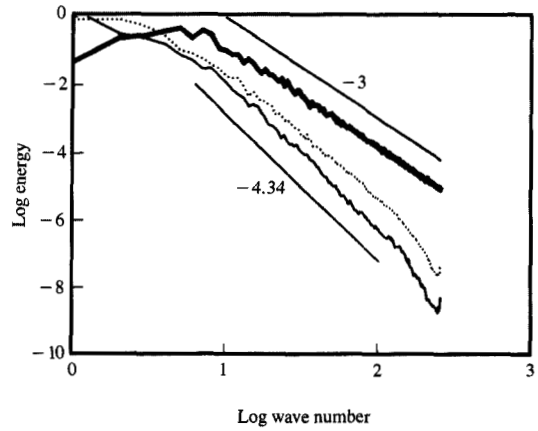

Figure 5

Time evolution of energy spectra. The plot shows how a turbulent flow, starting from a Kraichnan–Batchelor initial spectrum with $E(k) \sim k^{-3}$ and random phases, develops steeper and steeper spectra over time. The thick solid line is time $t = 0$, the dotted line is $t = 10$, and the thin solid line is $t = 40$. The normalization is $2\pi E = \int_0^\infty E(k)dk$.

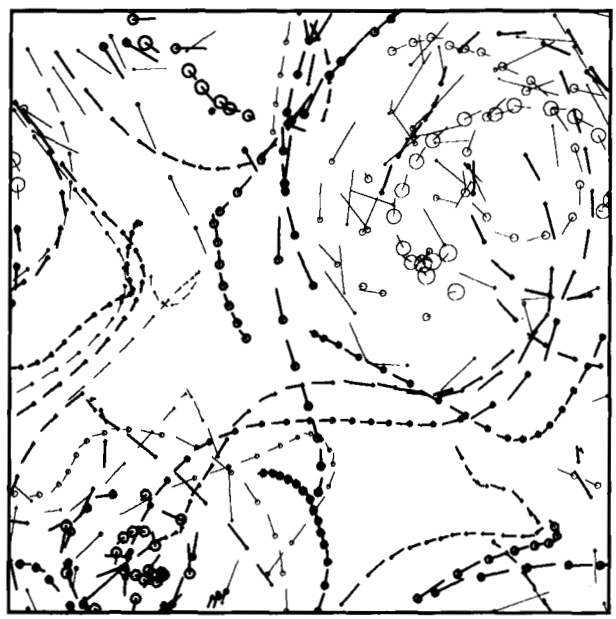

Figure 4

Vortex motion. The trajectories of the centers of the largest 25 vortices for the time interval 30–40. Thick and thin lines are used for positive and negative vortices, respectively. Circle sizes and segment lengths are proportional to vortex radii and velocities, respectively. The vortices are defined phenomenologically as those connected domains where $|\omega| \leq \omega_{threshold}$, with $\omega_{threshold} = 4$ and vortex area ≥ 0.01. During the represented time interval, two merging events take place, and the number of vortices decreases correspondingly. Note how vortex trajectories appear to be relatively smooth over long time scales, of the order of at least some time units; this is a remarkable phenomenon for a turbulent system. These times are much larger than other time scales such as the vortex *spinning time*, $T_{spin} \sim 0.15$; one also observes that small vortices tend to move faster than large ones. This representation shows a nice feature near the left side of the domain; a small-scale dipole forms and lasts for at least ten time units, showing approximately no interference due to the rest of the system; the videotape shows this phenomenon in great detail.

The most important clue that characterizes the deviation from the classical KB description is definitely given by the fact that an approximate relationship $\omega = \omega(\psi)$ is found for each vortex in the (ψ, ω) plane (**Figure 6**), thus indicating that all vortices are approximate solutions of the stationary nonviscous two-dimensional Navier–Stokes equation (7), $J(\psi, \omega) = 0$. Because of this important property, and since vortices contain the bulk of the total enstrophy, they can only account for a small amount of the total dissipation. In fact, since dissipation can act quickly only on small scales, large-scale structures such as vortices cannot dissipate appreciably. In other words, it happens that most of the total enstrophy is trapped in vortices and cannot flow toward small scales, thus inhibiting the main flow mechanism which is the basis of the KB theory (see **Figure 7**). On the other hand, the total enstrophy appears to decay in Figure 7, thus indicating that a KB enstrophy transfer mechanism really takes place, but only for the dynamically negligible nonvortex component of the field. This phenomenon is further illustrated in **Figure 8**, where one sees that the nonvortex component (reasonably defined as the domain where $|\omega| \leq \omega_{threshold}$) has a sharp k^{-3} spectrum, as predicted by the KB theory. All these remarks further support the idea that the fluid is really decoupled into two components, where the vortices play the leading role and drive the background component as if it were a passive scalar field [24].

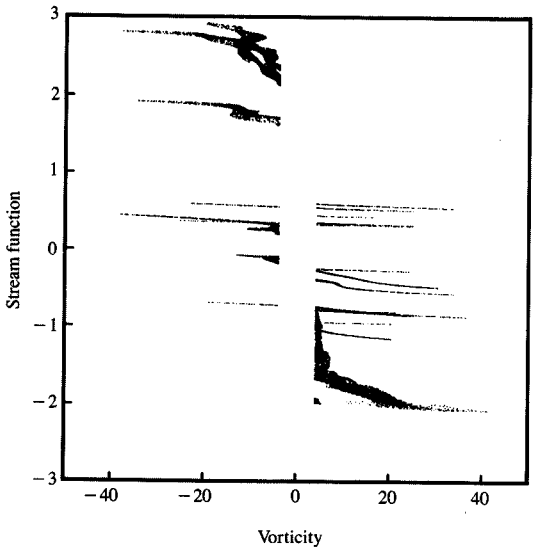

Figure 6

Coherent structures. Scatter plot of the stream function against the vorticity at time $t = 40$. Vortices are defined as in Figure 4; the stream function of each vortex is corrected for the velocity of the corresponding vortex center according to the simple relation $\psi' = \psi + u_y(x - x_0) - u_x(y - y_0)$. Each line corresponds to a single vortex; the plot indicates that the vortices are coherent structures, i.e., that they are solutions of the stationary nonviscous two-dimensional Navier–Stokes equation (7), $J(\psi, \omega) = 0$. Some of the largest vortices show thicker lines, primarily because they are strongly interacting with a neighboring one having the same sign, and the previous correcting term should be further modified to take rotation into account.

The high numerical resolution of the simulation produces a large number of vortices, most of them small-scale; **Figure 9** shows statistics for vortex radii. The main result is a quasi-self-similar statistical distribution, with

$$dN \sim R^{-1.98} dR. \tag{12}$$

This empirical formula is obtained from numerical simulation and is very probably the result of merging mechanisms. Indeed, a simple evolution equation for vortex populations undergoing merging events can be formulated and gives results similar to Equation (12) under very broad conditions [15]. These statistical results are of great importance because they cast a definitive light on the disagreement between the spectral slopes given by the KB theory and those found in numerical experiments. Indeed, under the reasonable assumption (proven in [15]) that all vortices have the same approximate radial profile, one can show that a self-similar statistical distribution $dN \sim R^{-\alpha} dR$ for the vortices implies a self-similar energy spectrum $E(k) \sim k^{-\beta}$, with $\beta = 6 - \alpha$ [15]. The application of this formula to our experiment gives $\beta = 4.02$, in reasonable agreement with the slope of the total spectrum $\beta = 4.34$ as in **Figure 10**; the same figure suggests a similar conclusion from a graphical point of view. In fact, the total spectrum appears to be the envelope of the spectra of the single vortices, while the background component is always negligible and does not appear to play any significant role in the total energy balance. In conclusion, the steep slope of the energy spectrum emerging from the numerical simulation appears to be a simple consequence of the statistical distribution of the vortex radii.

The final picture emerging from the numerical simulation is the following one:

- A hierarchy of coherent structures or vortices emerges from the random KB-like initial conditions, mainly as the result of coagulation processes such as merging.
- The vortices, though covering only a small fraction of the total area, are the main dynamic component of the system.
- Each vortex is an approximate solution of the inviscid stationary Navier–Stokes equation and thus cannot dissipate rapidly.
- The spectrum evolves through a series of self-similar and increasingly steeper stages.
- The statistical distribution of vortex sizes determines the slope of the energy spectrum and is, in turn, determined by simple evolutionary models for vortex populations which are based on merging.
- During the late stages of the dynamic evolution, the trajectories of the vortices are rather smooth, over many time units, in spite of the many small time scales that can easily be found in the system.

All of these conclusions suggest that the relevant dynamic variables of the system are the vortices and that the entire system can be decoupled into two main parts: 1) the driving mechanism, formed by the vortices, and 2) the rest of the field, which is passively advected by the vortices and shows a nearly classical KB-like behavior.

• *The influence of initial conditions and the breaking of scale invariance*

An important question arising each time one tries to derive physical results from numerical solutions is the dependency of the obtained results on the initial conditions. A second experiment on decaying turbulence is presented here in order to check such a dependency; its initial configuration is obtained from (11) with $\gamma = 6$ and $k_0 = 6$; this gives a steep spectrum, approximately $E(k) \sim k^{-6}$, and the corresponding configuration

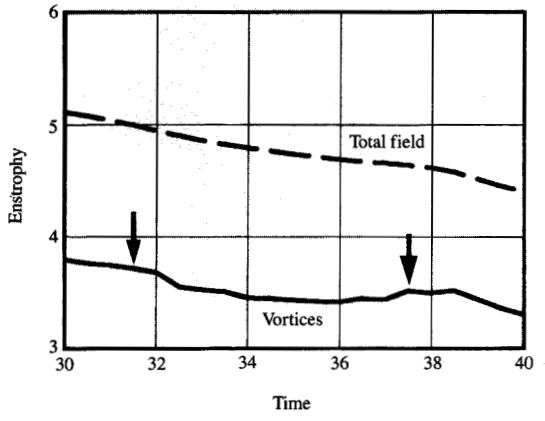

Figure 7

Enstrophy conservation. Enstrophy against time for the eight largest vortices (solid line) and for the total system (dashed line). The arrows indicate approximately the only two merging events that take place during the represented time interval. Each merging gives rise to a somewhat delayed enstrophy dissipation; this is a result of the dissipation of the filamentary structures arising from merging. Between merging events, vortex enstrophy tends to be conserved, while total enstrophy (dashed line) decreases monotonically.

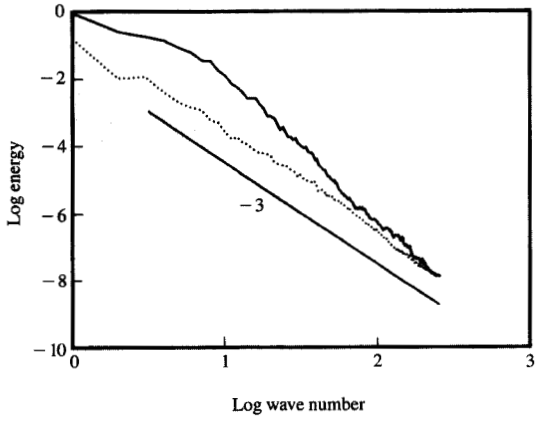

Figure 8

Spectrum of the background field. Energy spectrum of the vortices (solid line) and of the remaining part of the field (dotted line) at time $t = 40$. Note how the background component (defined by $|\omega| \leq 4$) shows a nearly Kraichnan–Batchelor spectrum and indicates a direct enstrophy cascade. This implies a corresponding enstrophy dissipation, in agreement with the dissipation observed for the nonvortex component of the field, as in Figure 7. The spectrum of the vortex component is much steeper and always dominates the background one.

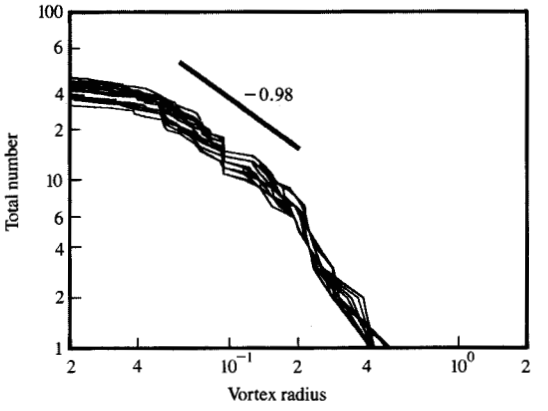

Figure 9

Vortex statistics: Integral of the vortex radius distribution function. Many plots are superimposed for different times in the range $t = 30$–40. Since the better-defined vortices are the large-scale ones, the integral $N(R) \sim \int_{R_{max}}^{R} \eta(R')dR'$ is defined from right to left. The slope of the fit is approximately $\alpha = -0.98$. One may wonder whether the indicated fitting interval and the corresponding slope are the proper ones. In fact, there are several reasons to restrict the fitting interval. First, the interval should not include the large-scale vortices, because a small number of vortices implies limited statistics. Second, a small-scale threshold must be used to avoid the inclusion of filamentary structures or spurious vorticity ripples. The lower radius threshold used for fitting (radius ≥ 0.06) corresponds to the area threshold (area ≥ 0.01) used to define vortices in all previous figures (see, e.g., Figure 4). The slope obtained by this fitting is roughly similar to the statistical result found in [15], where a self-similar distribution function is more evident and probably corresponds to a system which is dynamically much more evolved.

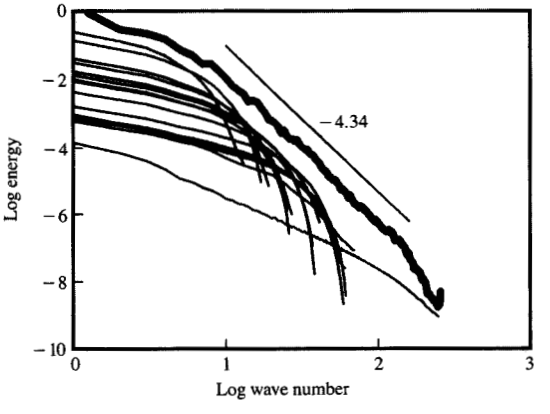

Figure 10

Spectra of single vortices. Energy spectra of the 15 largest single vortices (thin solid curves) and of the total vorticity field (thick solid curve). It is readily seen that the vortices are the dominant dynamic component. The vortices clearly determine the power-law index $\beta = 4.34$ of the total energy spectrum.

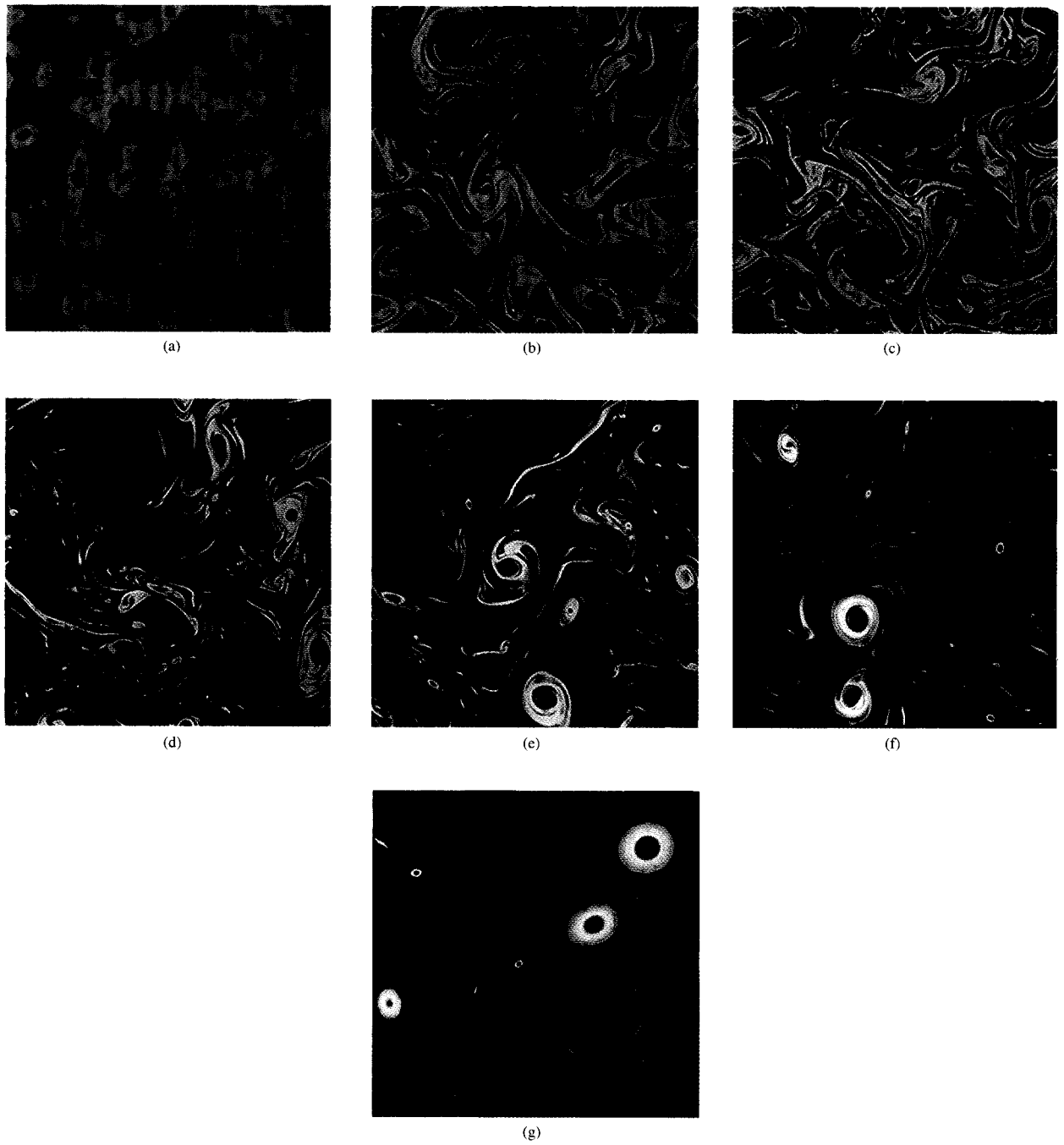

Figure 11

Decaying turbulence simulation with a steep initial spectrum. Instantaneous vorticity fields at times $t = 0$ (a), $t = 2$ (b), $t = 5$ (c), $t = 10$ (d), $t = 15$ (e), $t = 20$ (f), and $t = 40$ (g). The color table is as in Figure 1. Starting from a steep spectrum $E(k) \sim k^{-6}$, despite the random phases, only few degrees of freedom are really excited, and the initial state (a) is much more regular than in Figure 1(a). Over time, the initial large-scale vorticity patches are stretched [(b) and (c)] and the resulting vorticity filaments tend to break into small-scale vortices, mainly as the result of inviscid instabilities [(c) and (d)]. Eventually, (e) and (f) follow approximately the scenario described by the late evolution of the system shown in Figure 1. All the parameters of the simulation, including superviscosity, are the same as in Figure 1.

[**Figure 11(a)**] appears to be a rather regular one with well-identified and large-scale vorticity patches. The interest for such initial conditions is intrinsic because they are very different from the ones studied previously; moreover, the use of steep initial spectra has been triggered by the appearance of some numerical

experiments [25–27], indicating that this class of initial conditions really decays into a more classical KB-like spectrum.

To study the influence of steep initial spectra more extensively, a very high-resolution (1024 × 1024) experiment [10] was integrated for a very long time. Here we present a similar experiment at lower resolution (512 × 512), in order to be comparable with the previous one, again with the aid of the videotape recording technique. Similarly, superviscosity is used, with $p = 2$ and $\nu = 2 \times 10^{-9}$. The experiment confirms the scientific results indicated in [10], namely that a spectrum $E(k) \sim k^{-3}$ is really developed, but only as a transient stage before a steeper asymptotic spectrum is obtained. This previously unreported experiment also shows that it is not necessary to use a huge spatial resolution to demonstrate the scientific contents shown in [10]. The numerical parameters and the total integration time are the same as in the previous experiment.

Figure 11 shows the dynamic evolution of the system. As already observed, the initial conditions of the experiment exhibit large vorticity patches with sizes close to the half-wavelength $l_0 \sim \pi/k_0$. The dynamic evolution almost immediately shows the formation of elongated vorticity sheets (as shown in [25] or [26]), mainly as the consequence of stretching mechanisms; at the same time one observes the formation of a full inertial range similar to the one predicted by the KB theory [see **Figures 11(b)** and **12**]; this corresponds to a fast accumulation of power at small scales and, in turn, gives a direct enstrophy cascade, again according to the KB theory. Successively, around time $t = 5$–10 [**Figures 11(c)** and **11(d)**], the appearance of the field begins to change, and a number of well-formed, large-scale vortices with size of order l_0 appear to be embedded in a complex background. The tape animation shows how each large-scale vortex can be traced back to a vorticity peak in the initial configuration, so that this system appears to maintain a remarkable memory of the initial conditions.

Around $t = 10$, Figure 11(d) shows that the previous filamentary background now contains many small-scale vortices. The videotape shows these to be the result of multiple breakings of the vorticity filaments or the outcome of complex inviscid instabilities.

A global measure of the turbulent activity of a two-dimensional system is considered to be the palinstrophy, defined as

$$P = \frac{1}{2A} \int (\bar{\nabla}\omega)^2 \, dxdy = \int_0^\infty k^4 E(k) \, dk. \qquad (13)$$

Figure 13 shows the time evolution of the energy, enstrophy, and palinstrophy. The rapid increase of palinstrophy clearly indicates how the evolution that takes place during the first five time units has a substantially inviscid character, in agreement with the observed formation of small-scale structures. The final result is that the fluid flow is dominated by two populations of vortices. The first comprises all large-scale

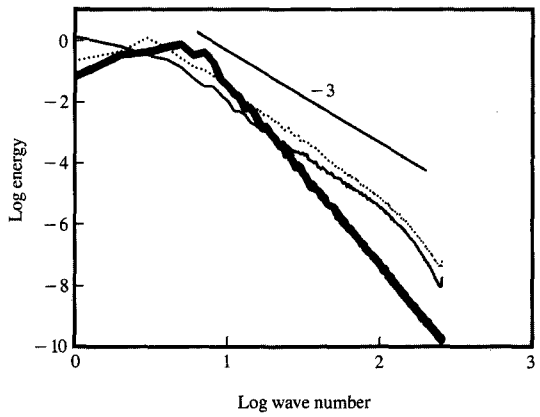

Figure 12

Time evolution of energy spectra. Energy spectrum $E(k)$ of the flow at time $t = 0$ (thick solid line), $t = 2$ (dotted line), and $t = 10$ (thin solid line). Note how the initial intense vortex-stretching activity quickly accumulates power at small scales. All energy spectra in the range $2 \leq t \leq 10$ have slopes similar to the one predicted by the Kraichnan–Batchelor theory, but the corresponding configurations [shown in Figures 11(b), 11(c), and particularly 11(d)] differ considerably.

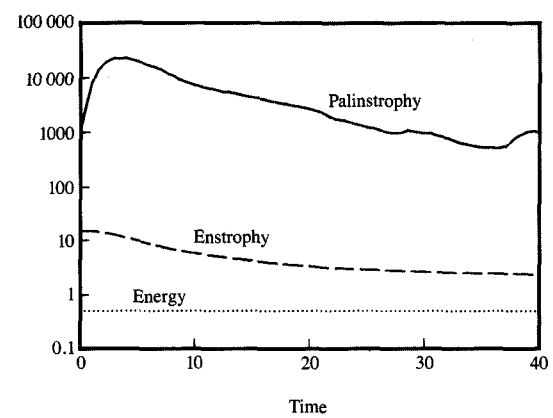

Figure 13

Initial increase of turbulent activity. Energy E (dotted line), enstrophy Ω (dashed line), and palinstrophy P (solid line) as a function of time for the entire run of the experiment.

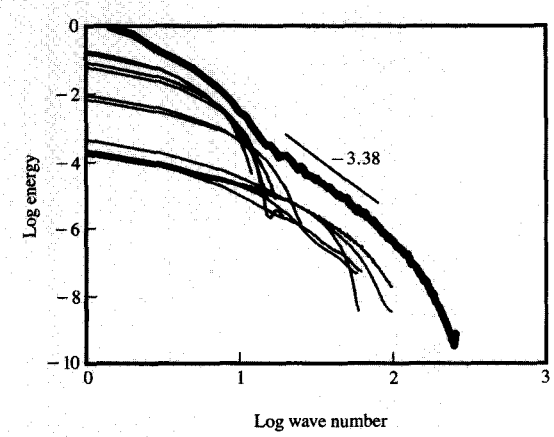

Figure 14

Non-scale-invariant spectrum. Energy spectra of the largest vortices (thin solid curves) and of the time-averaged energy spectrum of the total vorticity field for $25 \leq t \leq 35$ (thick solid curve). Vortices are defined as in Figure 4. Although vortices are still the dominant dyamic component of the system, as in Figure 10, the spectrum is no longer scale-invariant. The vortices clearly belong to two different populations. The large-scale population is a remnant of the initial condition, while the small-scale one forms during the repeated fragmentations of the many vorticity filaments which develop almost immediately after the start of the simulation (see [10]).

vortices, and the second contains the remaining small-scale vortices, formed by the fragmentation of the vorticity filaments. Subsequently, a more classical decaying phase begins and dominates the evolution; merging events are the only mechanism which is able to fill the gap between the two populations of vortices, while some small-scale vortices may be dissipated on short (advective) time scales due to the intense stretching fields of the large vortices.

The spectrum resulting from the late time evolution steepens increasingly with time and is shown in **Figure 14**. The most striking feature is the lack of scale invariance (see Figure 10); the total spectrum again appears to be the envelope of the spectra of the single vortices, which are here recognizable as clearly grouped into two separated populations.

An important tool that can be used to describe the "state" of a turbulent system is due to Novikov [28] and is given by the so-called *centers of gravity*, K_v and K_Ω, for the velocity and vorticity respectively; they are easily defined by

$$K_v = \frac{\int_0^\infty kE(k)dk}{\int_0^\infty E(k)dk},$$

$$K_\Omega = \frac{\int_0^\infty k^3E(k)dk}{\int_0^\infty k^2E(k)dk},$$

$$K_0^2 = \frac{\int_0^\infty k^2E(k)dk}{\int_0^\infty E(k)dk}, \tag{14}$$

where K_0 is a conserved quantity for an inviscid flow. A system that evolves according to a classical KB scenario should contemporarily show a direct cascade for enstrophy and an inverse one for energy; the correspondingly Novikov centers of gravity should respectively increase and decrease with time. **Figure 15(a)** shows a clear direct enstrophy cascade, but only during the first five time units, followed by a more classical decay phase; in **Figure 15(b)**, which shows the simulation that starts with the k^{-3} spectrum, no such initial transient appears.

Summarizing the results of the two experiments on decaying turbulence, one sees that the initial conditions are very important and that they influence the full system, at least on time scales like the ones we have investigated. Moreover, a steep spectrum induces a new, nearly classical, KB-like transient phase that develops into a non-self-similar asymptotic phase. This suggests that a threshold value should exist that separates the scale-invariant evolution observed with initial flat spectra [such as $E(k) \sim k^{-3}$] from the more complex behavior given by steep initial spectra.

3. Three-dimensional flows

The high-resolution simulation of three-dimensional flows is the current challenge for numerical fluid dynamics. From the theoretical point of view, the difficulties of the problem are shown by the same basic statistical theories which indicate that the three-dimensional problem is much more complex than the two-dimensional one. In fact, the intrinsic number of turbulent degrees of freedom is much larger, not only as a consequence of the existence of the third dimension but also because the dynamics are expected to be much more complex. The last point is clarified by the fact that the Kolmogorov spectrum [three dimensions, $E(k) \sim k^{-5/3}$] is unfortunately much flatter than that described by Kraichnan and Batchelor (two dimensions, $E(k) \sim k^{-3}$]; in other words, three-dimensional dynamics *extend* over a much wider range of scales.

The traditional and still most powerful simplification of the problem assumes that it is not possible to study numerically the many small scales of the system; some *physically reasonable* theory must consequently be used to simulate their behavior. Among the various attempts, we cite *eddy-viscosity* models (see, e.g., [29]) and *subgrid-scale* models (see [30] for a review), which are used to

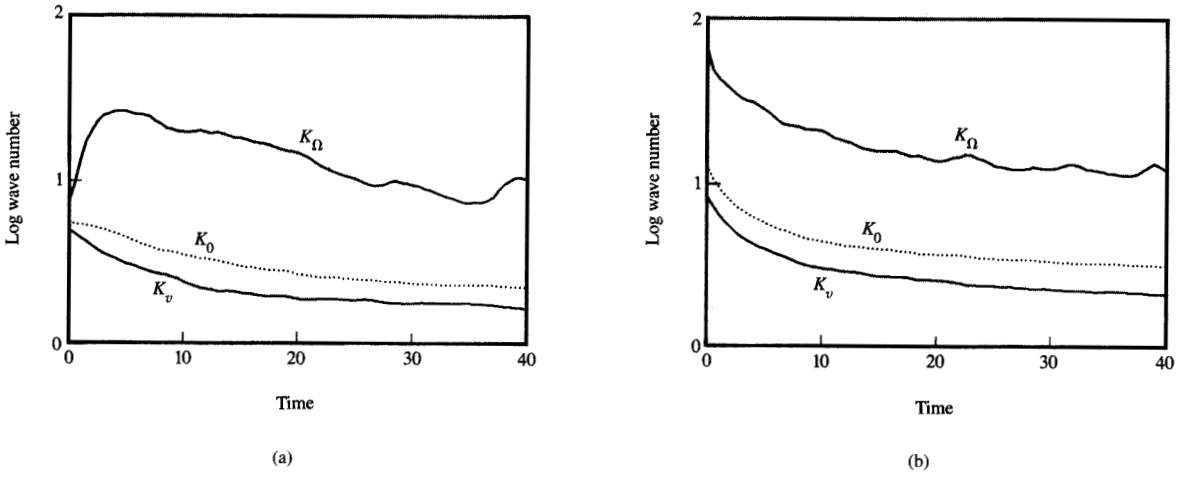

Figure 15

Initial inviscid behavior. Time evolution of Novikov's *centers of gravity* K_v (velocity), K_Ω (vorticity), and K_0 as defined in Equation (14). (a) Initial inviscid behavior. The flow that starts with a steep spectrum behaves like an inviscid flow during the first five time units. In fact, the vorticity wave number increases during the first part of the simulation, thus suggesting an initial direct enstrophy cascade. No such behavior is shown in (b), the simulation that starts with a flatter spectrum $E(k) \sim k^{-3}$.

simulate the nonlinear energy transfer and dissipation that should take place on unresolved scales. All these theories, also referred to as *closure theories*, have a strong phenomenological character and are generally based upon some reasonable assumptions. In any case, it is clearly difficult to compress into synthetic laws the detailed dynamics that should take place over a very wide range of scales. One of the most recent and promising theoretical developments is given by the application of the renormalization group technique (proposed in [31]) as a new tool with which to approach the closure problem for the Navier–Stokes equation (see also [32]).

A formulation of the Navier–Stokes equation for three-dimensional incompressible viscous flows, particularly well suited for the numerical integration, is given by

$$\frac{\partial \bar{u}}{\partial t} = \bar{u} \times \bar{\omega} - \bar{\nabla}\left(\frac{p}{\rho} + \frac{1}{2}u^2\right) + \nu\Delta\bar{\omega} + \text{forcing}; \qquad (15)$$

this is obtained by simply substituting the vector identity (3) in (2) [16]. As already discussed in Section 1, the main fluid-dynamic content of (15) is inside the nonlinear part, which is best shown in Equation (4) where it clearly contains two parts: a vorticity advection component and a *vortex stretching* component (see, e.g., [2]), which is a mechanism that tends to elongate vorticity tubes.

From the numerical point of view, the three-dimensional fluid dynamics problem is at present severely limited, not only by traditional bounds on computer memory and computational power, but also by the graphical representation of the three-dimensional computer results, because of the need for simple and fast tools to show the significant flow patterns. This is of particular importance, since it is expected that three-dimensional as well as two-dimensional flows could be dominated by easily recognizable coherent structures (i.e., the inviscid solutions of the stationary Navier–Stokes equations), even though these have not yet been defined nor observed in detail (see [33] for an extensive review, and also [34] for a more critical assessment). Interest in the existence of coherent structures is dictated by their nature; in fact, these could strongly inhibit the energy cascade, thus changing substantially the global Kolmogorov scenario. Some numerical and laboratory evidence, supporting the presence of coherent structures in three-dimensional flows, has been reported by many authors and is based on the generally accepted assumption that, although *vortex stretching* may tend to destroy any initial large-scale flow, the dynamic evolution continuously tends to produce a dynamic hierarchy of structures (see [35] for an extensive review).

Equation (15) contains two nonlinear terms and thus shows the complexity of any attempt to classify the inviscid stationary solutions of the flow equations. On the other hand, it is clear that a quantity such as the alignment (*cosine of the angle*) between velocity and vorticity must play a significant role in such a classification. In fact, any significant parallelism or

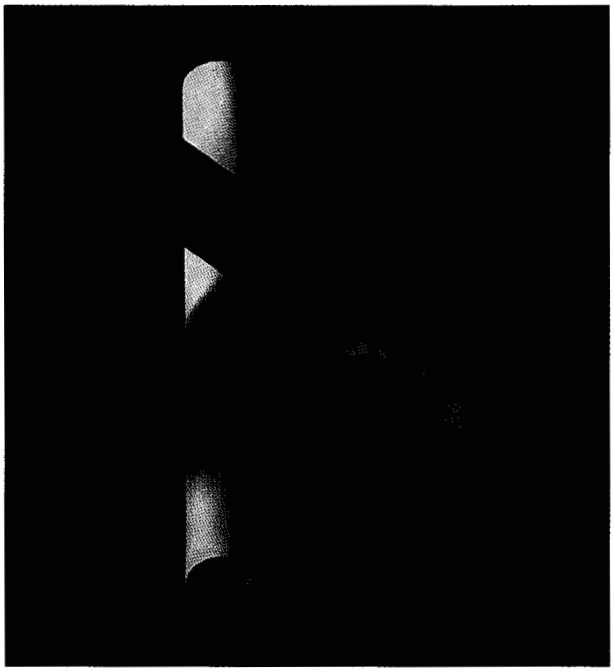

Figure 16

Two orthogonal vortex tubes, case 1. The initial condition of the experiment is represented by isovorticity surfaces; the vorticity value is $|\omega| = 12$. The two vorticity tubes are initially orthogonally offset and differ only in their radius, the foreground tube being slightly larger than the background one. The observation direction is defined in terms of the standard Euler angles: $\phi = 45$, $\theta = -45$, $\xi = 0$. The computation has been performed using a de-aliased pseudospectral code; the side of the cubic box is 2π, the grid size is $128 \times 128 \times 128$; superviscosity is used, with $p = 2$ and $\nu_2 = 2.625 \times 10^{-5}$; the time-step is $\Delta t = 3.7 \times 10^{-3}$; and time evolution is performed for 700 time-steps. The three-dimensional rendering of the simulations is obtained on an IBM 6090 Graphics System with the aid of the IBM graPHIGS Programming Interface using the *Marching Cubes* algorithm to approximate the isovorticity surface; the software interface is the ECSEC visualization tool. The surface is colored according to the intensity of the velocity on the surface. One ambient light and three different directional lights are used to brighten the scene and cast shadows.

antiparallelism between these vectors implies a negligible value of the cross-product $\bar{u} \times \bar{\omega}$ and consequently indicates the existence of a local approximate solution of the inviscid and stationary equation (15).

Zabusky and Melander [36–38] have recently proposed some numerical experiments that start from two orthogonally offset vorticity tubes, in a simple cubic box with periodic boundary conditions, to study how some interesting types of three-dimensional instabilities develop from simple initial conditions. These simulations, though apparently simple, avoid the complexity of starting from a more general initial configuration and still retain many of the important but poorly understood properties of three-dimensional flows. They address the problem of initial tube stretching and the possibility of a later reconnection, and conclude that no real reconnection is to be expected (at least on short time scales), but rather a complex entanglement of the initial vorticity tubes [36]. All of these experiments are a good example of the difficulties of the numerical three-dimensional problem, since not only powerful computers are needed but also a sophisticated graphical output. Melander and Zabusky almost always used three-dimensional isovorticity surfaces to present the dynamic behavior, but it is clear that any advance in the field of graphical representation must be considered as remarkable progress. Here we repeat and complement some of their experiments with the aid of a time-dependent videotape animation; different observation angles are used to enrich the spatial comprehension of the configurations. This turns out to be considerable progress, since it avoids the storage of prohibitive amounts of three-dimensional data, but the selection of a given type of field (e.g., vorticity and not velocity) or of a given value of isosurface drawing still strongly constrains any further analysis of the dynamics.

Since we confine all our experiments to a simple cubic domain, the numerical integration method is simply based on the well-known and efficient pseudospectral technique; the evaluation of the right-hand side of (15) uses a two-step procedure consisting of time evolution according to the shortened equation

$$\frac{\partial \bar{u}}{\partial t} = \bar{u} \times \bar{\omega} + \nu_p \Delta^p \bar{u}, \tag{16a}$$

(which generally produces a non-divergence-free flow) and removal of the compressible component of the field using

$$\hat{\bar{u}}_{\text{divergence free}} = \hat{\bar{u}} - \frac{\bar{k}}{k^2}(\bar{k} \cdot \hat{\bar{u}}), \tag{16b}$$

where $\hat{\bar{u}}$ is a Fourier component of $\bar{u}$; the entire procedure is easily shown to be fully consistent with Equation (15) [16]. Note how we generalize for superviscosity as in Equation (7). De-aliasing is obtained by averaging over two half-mesh-shifted grids and truncating inside a sphere defined by $K^2 \leq 8/9 K^2_{\max}$ [16]; time evolution is performed as for the two-dimensional case, and the numerical code has been fully vectorized and parallelized under MVS/XA using MTF (MultiTasking Facility [19]). The side of the cubic box is 2π, the numerical resolution is $128 \times 128 \times 128$; the superviscosity parameters are $p = 2$, and $\nu_2 = 2.625 \times 10^{-5}$; the time-step is $\Delta t = 3.7 \times 10^{-3}$, and time evolution is performed for 700 time-steps.

Here we present a couple of numerical experiments, case 1 and case 2, in which the initial condition,

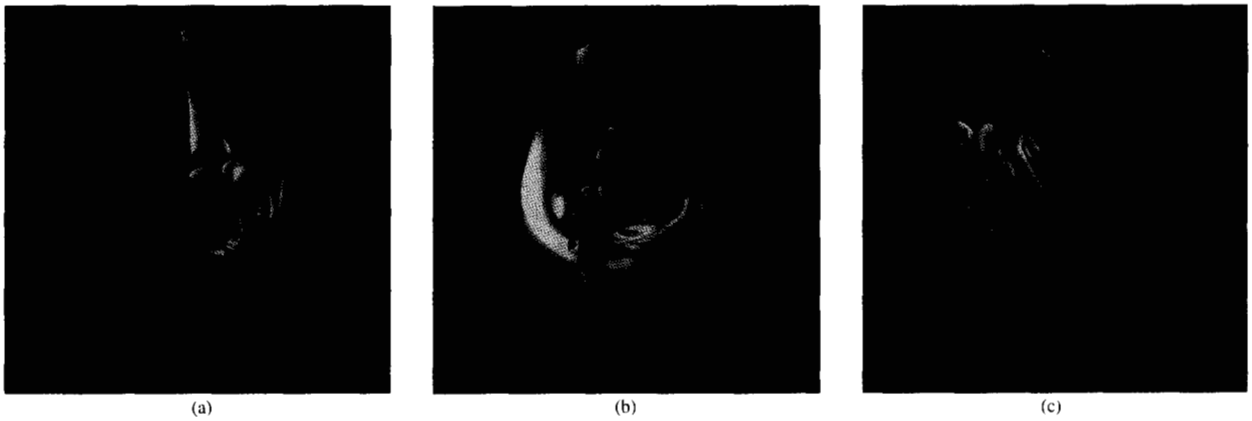

(a) (b) (c)

Figure 17

Entanglement of vortex tubes, case 1. Time $T = 1.5$. The time evolution of two initially orthogonally offset tubes produces the concurrent development of many instabilities. The same configuration is shown from three different observation angles (a), (b), and (c). The two original tubes, though highly distorted, appear to be well isolated, particularly in (c), and show no sign of reconnection; the configuration shown here displays many small-scale secondary vortex tubes that bridge the gap between the main tubes. In reality, the terms *isolation*, *reconnection*, and *secondary vortex tube* are highly misleading and are an artifact of the representation; in fact, no vortex reconnection takes place, but rather a complex vortex entanglement, as is clearly shown in a previous computation by Melander and Zabusky [22]. The observation angles are (a) $\phi = 0$, $\theta = -90$, $\xi = 0$, (b) $\phi = 45$, $\theta = -45$, $\xi = 0$, and (c) $\phi = 135$, $\theta = 45$, $\xi = 0$. Since the coloring is given by the intensity of the velocity field, one understands quickly the dynamic behavior of the system. The blue parts of the vorticity isosurfaces indicate a slow velocity and hence a correspondingly slow motion of the fluid, and are generally connected to secondary structures arising from the instabilities due to the nonlinearity of the equations. Conversely, the red surfaces indicate rapidly moving fluid components and are generally associated with the original main vorticity tubes. The maximum values of the vorticity and velocity fields are here $|\omega| \sim 50$ and $|u| \sim 6$, respectively.

representing the orthogonally offset tubes of Melander and Zabusky, is given by

$$\bar{\omega}(\bar{r}) = \omega_{01} \exp\{-l_1^2[(y - \pi/3)^2 + z^2]\}\bar{e}_x + \omega_{02} \exp\{-l_2^2[x^2 + y^2]\}e_z ; \quad (17)$$

for case 1 the parameters are $\omega_{01} = \omega_{02} = 20$, $l_1 = 3^{-1/2}$, and $l_2 = 0.5$; for case 2, $\omega_{01} = 20$, $\omega_{02} = 5$, and $l_1 = l_2 = 3^{-1/2}$.

• *Discussion of the numerical experiments*

The dynamic evolution of case 1 is the more interesting of the two presented experiments, because initially the two tubes are approximately equivalent (**Figure 16**) and their time evolution is expected to affect both of them strongly. At the beginning of the simulation, a highly symmetric and nonlinear deformation appears near the point of maximum closeness; this quickly develops into a much more complex configuration. At the same time many well-detached thick curvilinear vorticity tubes show up near the center of the cubic domain, bridging the gap between them (**Figure 17**). These structures tend to increase in size and, in turn, give rise to other smaller structures. The literature contains many names to indicate structures such as those observed: *vortex filaments*, *vortex rings*, *hairpins*, *rolls*, *bridges*, or *ribs*, and different terms for the possible dynamic phenomena such as *reconnection*, *entanglement*, *threading*, *cross-linking*, or *cut-and-reconnection* (see, e.g., [36–39]). The wide taxonomy of these terms reflects the great complexity of the three-dimensional problems and also indicates that much progress has yet to take place in the comprehension of the dynamics as well as the graphical representation of the data.

The most interesting phase of this simulation occurs approximately between times 1.5 and 2.5. During this interval, it appears that the secondary structures that roll up the two main tubes tend to squeeze them and to grow thicker, so that around time $t = 2.5$ an apparent *cross-reconnection* happens (compare Figure 17 with **Figure 18** and observe in detail the tape animation); this raises a justifiable concern about the possible development of a flow singularity and about the consequent accuracy of the numerical model. Melander and Zabusky [36] have discussed this problem in detail and have reached the reasonable conclusion that simulations such as the one reported here are numerically accurate enough, but that no reconnection and no singularity really take place on these time scales. Rather, an increasingly complex vortex entanglement is seen. They argue that, even though unresolved small scales could in principle be excited during the apparent reconnection, there is no time for

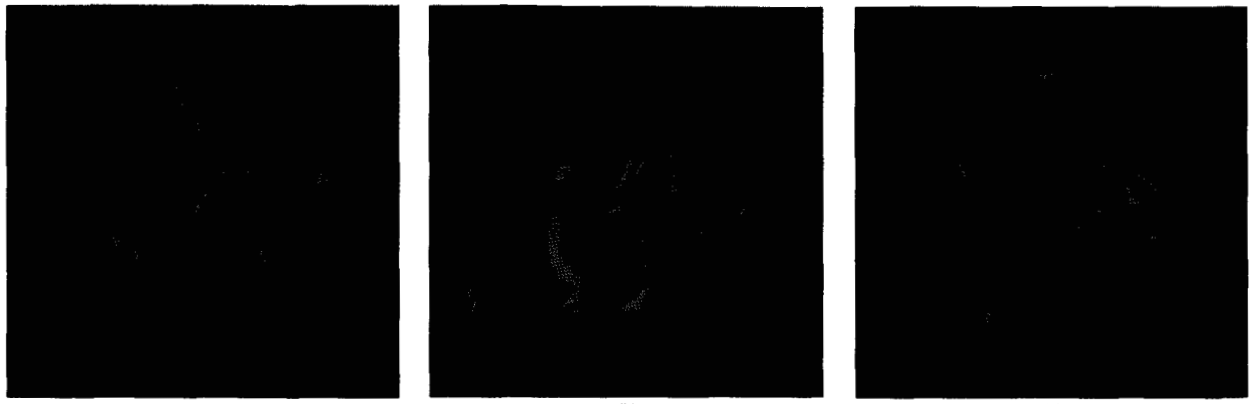

(a) (b) (c)

Figure 18

Three views of the "reconnection" of vortex tubes, case 1. Time $T = 2.6$. The same simulation as in Figure 17 but at a later time, when the apparent tube reconnection has already taken place.

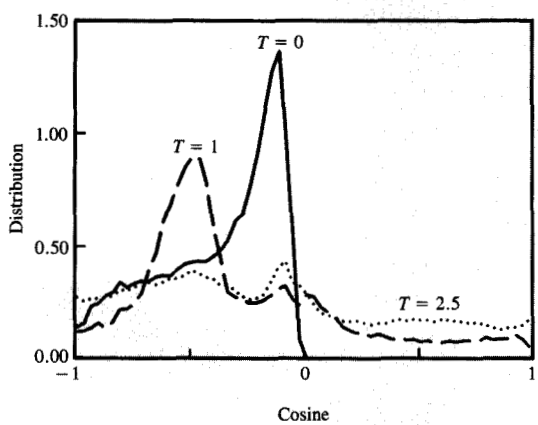

Figure 19

Cosine distribution, case 1. Normalized probability distribution of the cosine of the angle between velocity and vorticity for all cells where $|\omega| \leq 12$. The maximum of the distribution tends to shift to the left with time, up to the apparent tube reconnection, indicating how the tubes tend to become more and more antiparallel. After "reconnection" the distribution flattens. The numerical parameters are the same as indicated in Figure 16.

any feedback on the tubes, which are large-scale structures. Note how the ultimate evolution of the flow loses any trace of the initial order and tends to show an increasingly chaotic behavior.

The only attempt to analyze the flow mathematically is done here in terms of the cosine diagnostics that we have discussed previously to identify a possible degree of coherency inside the flow. Each initial vorticity tube is clearly a *coherent structure*, at least from the pictorial point of view, but is unfortunately characterized by the orthogonality of the velocity and vorticity vectors, thus eluding the cosine diagnostics itself; nevertheless, during the dynamic evolution, a temporary helical negative correlation of velocity and vorticity shows up (**Figure 19**), indicating an *antiparallel* phase and the presence of some degree of coherence inside the flow. This coherence fades away after the "reconnection."

The initial conditions of case 2 are very different, because the secondary tube is much fainter than the primary one (**Figure 20**). The dynamic evolution is correspondingly simpler because the main tube is only slightly perturbed during the entire run of the experiment. The only rapidly evolving component is the secondary one, which is in turn continuously dragged and stretched around the primary tube (**Figure 21**). Later, the secondary vortex continues to circulate around the main one while extending its influence further and further from the central symmetry plane of the main tube. Near the end of the simulation, two small-amplitude ridges appear to travel in opposite directions on the surface of the main tube; these are located on the lateral edges of the complex formed by the circulating secondary tube and are excited by its squeezing action (see the tape animation).

4. Visualization techniques and the animation tool

We have used two different visualization techniques for our two examples; the difference is due to differences in the dynamic phenomena of interest. The visualization effort is also very different for two- and three-dimensional

calculations because of the different quantities of data produced for the two cases and the different techniques adopted to display the dynamic quantities.

In numerical experiments on two-dimensional turbulence, it is widely accepted that the vorticity field is the most informative quantity to investigate (see for example [2] and [3]); this is not surprising also because the vorticity is a conserved quantity along the stream lines of an inviscid two-dimensional flow. Many papers report the results of computations using isovorticity contours, which work well in identifying the formation and evolution of coherent structures having a rather regular and clear appearance, even for high-resolution numerical computations.

On the other hand, contours are difficult to use while investigating the properties of noncoherent structures such as the background field, which has a low vorticity value, or the vorticity filaments that are observed when starting with smooth initial conditions. This happens because of the extremely complex nature of the low-vorticity structures; in these cases, contour plots are not sufficiently informative, or are blurred by many small-scale features.

A much more useful technique in the latter case is the use of a color lookup table, which equally renders low- and high-vorticity areas of the field and leaves the evaluation of the picture to the strong capabilities of the human eye. The lookup table translates vorticity intensities into three 8-bit numbers for the three different intensities of the red, green, and blue components so that an RGB image can easily be displayed. Our lookup table is managed by the same FORTRAN program that handles the numerical experiments and writes three RGB files; the pictures are displayed using the IBM Image

Figure 20

Two orthogonal vortex tubes, case 2. Isovorticity representation of the initial condition of the experiment. The parameters of the numerical experiment are here identical to those indicated in Figures 16, 17, and 18. The secondary background tube is not visible here because its maximum vorticity is below the represented vorticity level, $|\omega| = 6$. The standard Euler angles defining the observation direction are $\phi = 45$, $\theta = -45$, $\xi = 0$.

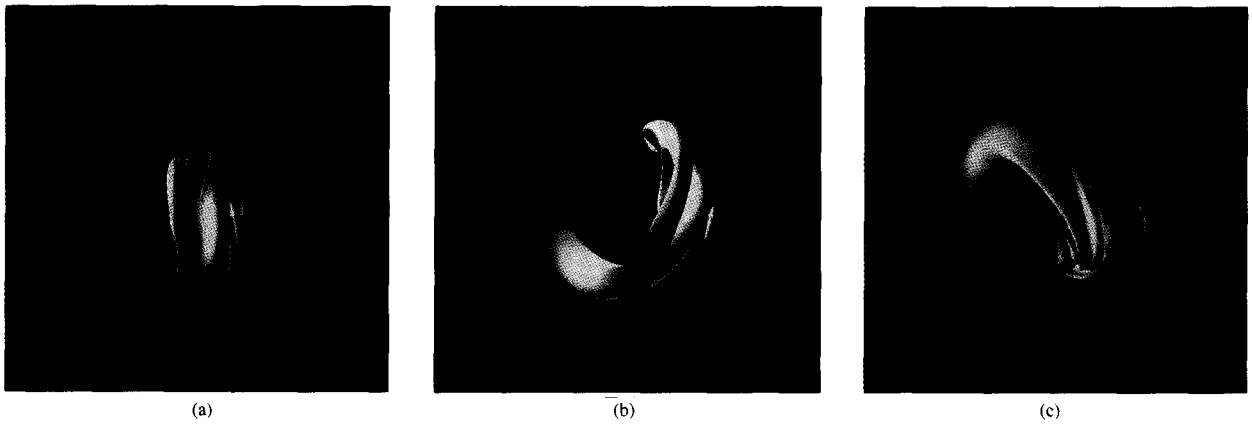

(a) (b) (c)

Figure 21

Entanglement of vortices, case 2. Time $T = 1.5$. The small vortex tube is now visible above the vorticity threshold $|\omega| = 6$ because its strength has been increased by the continuous circular dragging due to the large tube; at variance with case 1, here the large vortex is only slightly perturbed by the secondary one. The videotape shows tube stretching and compression of the large tube. The three observation angles are (a) $\phi = 0$, $\theta = -90$, $\xi = 0$, (b) $\phi = 45$, $\theta = -45$, $\xi = 0$, and (c) $\phi = 135$, $\theta = 45$, $\xi = 0$. Note how the slowly flowing green and blue parts of the isovorticity surface are generally connected to the secondary tube, which continuously generates more and more complex structures.

Access Executive (IAX) [40] with a variety of methods and devices, including the IBM 5080 Graphics System for photographic acquisition, and standard terminals such as the 3179 for monitoring the numerical calculations.

We have found very useful a "standard" lookup table for vorticity, where blue and red indicate clockwise and counterclockwise rotation respectively, while low-vorticity features are strongly enhanced empirically by using light-blue, green, and white. This has proven to be particularly effective because the observer can focus his attention on the desired structures by selecting the color. Figures 1, 2, 3, and 11 were obtained with this lookup table and are full-resolution reproductions of the original simulation.

An important component for the comprehension of the dynamic phenomena is time. This can be included if a video animation is produced; it is our opinion that this new and attractive way of presenting the results of the numerical computations will gain more and more momentum because of its intrinsic ability to display the results quickly. This opinion is validated by the fact that an increasing number of journals offer videocassettes in addition to the technical papers. This issue of the *IBM Journal of Research and Development* is an example of this new publishing technique; we can also cite [41] as another example where scientific results have been complemented by videos.

The video animations of the numerical simulations were obtained through the use of the two-dimensional-turbulence FORTRAN simulation program that periodically dumps on mass storage a temporary copy of the three RGB components of the vorticity field and sends them to a VM virtual service machine that manages the recording of the analog color video images. This virtual machine receives the data and sends them to an IBM AT Personal Computer running a program that contemporarily manages the RS-232C command interface to a SONY LVR6000/LVS6000[4] laser videodisk recorder and a VISTA[5] card that provides the translation of the RGB components into a video signal. Since the laser videodisk is a random-access device, it is worthwhile to note that this method easily allows for the video recording of data coming from different numerical experiments. In fact, the virtual service machine makes no distinction as to the sender of the data, which may be any user on any operating system (e.g., another remote VM, MVS, or AIX[6]) connected to the network, provided that a unique network data format is used. Besides recording, a useful set of general commands can be sent to the VM service machine: These include a request for a listing of the recorded frames or a request for a playback of some animations for the observation or the reversal of a standard videotape recorder. Our multi-user videodisk recording complex will be reported in more detail elsewhere [42].

Three-dimensional flows are a challenge for currently available visualization techniques; one can safely state that no conclusive method is yet known. Three-dimensional scalar fields are manageable, since the two-dimensional concept of iso-intensity contours can be extended to three-dimensional iso-intensity surfaces, at least from the conceptual point of view. However, three-dimensional vector fields cannot be represented easily, unless they are sufficiently smooth or are described by a low number of *effective* degrees of freedom. In the general case, a sufficiently accepted way of representing a three-dimensional vector field consists in plotting the iso-intensity surfaces of the modulus of the field together with a *color* that represents the local intensity of a second three-dimensional scalar field. This is a relatively viable procedure because *two* related quantities, out of the *three* components of the required vector field, are represented concurrently. On the other hand, there exist much more imaginative solutions, such as those presented in the well-known video on the numerical simulation of tornadoes, produced by the NCSA Visualization Production Team of the University of Illinois at Urbana (see, e.g., [41]).

All visualizations of the three-dimensional flows presented in this paper are based on the representation of iso-intensity surfaces of the modulus of the vorticity field and are colored according to the value of the modulus of the velocity field on the surface. The color table used to represent the velocity was chosen according to the *rainbow* rule. This shows blue and red for low and high velocity respectively; correspondingly, the green and all the other intermediate rainbow colors refer to intermediate velocity values. In three dimensions it may certainly be argued that isovorticity surfaces are not the best candidates to represent the results. Nevertheless, this is the solution used most often to date, at least in the case of incompressible flows. See also [43] for another example of representation of a similar numerical experiment.

The construction of the isovorticity surface is done at run time by a FORTRAN subroutine that builds a set of triangles approximating the desired surface according to the *Marching Cubes* algorithm [44]. This algorithm has the advantage of being very simple and effective, since it analyzes the computational lattice on a cell-by-cell basis and is parallelizable. Moreover, it is very fast because it is based on a simple lookup table that directly determines the number and the intersections of the triangles contained in each computational cell.

The production of the final rendition of the three-dimensional flow is based on the three-dimensional

[4] SONY LVR6000/LVS6000 is a trademark of SONY Corporation.
[5] VISTA is a trademark of TrueVision Inc.
[6] AIX is a registered trademark of International Business Machines Corporation.

graphical capabilities of the IBM 6090 Graphics Systems. These are exploited using the graPHIGS[7] 2.1 Programming Interface [45, 46], which allows the user to easily exploit the hardware of the IBM 6090 Graphics System for complex functions such as hidden-line removal, hidden-surface removal, lighting and shading effects, surface transparency, and depth cueing, in addition to simpler functions such as rotations and translations.

A user-friendly interactive environment that exploits graPHIGS 2.1 has been developed at ECSEC to fully analyze any combination of many-colored scalar fields over different and generally unconnected grids. The three-dimensional numerical simulation program has produced three different videos, corresponding to three different observation directions, using a FORTRAN interface to the above-mentioned ECSEC Visualization Environment. The three-dimensional videos were produced by reading the IBM 6090 frame buffer, using graPHIGS, and sending the red, green, and blue components directly to the videodisk service machine while the computational program continues its execution.

5. Conclusions

This paper is intended to show how videotape animation can enrich the comprehension of numerical simulations of two-dimensional turbulence and three-dimensional flows.

The scientific results obtained for two-dimensional turbulence are supported by a large body of graphical data, derived mainly from a sophisticated mathematical analysis of the numerical simulations (see [5, 8–10, 15]). On the other hand, the newly adopted method of analog color video recording appears to be a breakthrough, because many of those results can be perceived at a glance, just by playing the videotape. This is particularly evident not only for simple understanding of the time-dependent formation of the vortices (and the related merging events) but even for the more complex comprehension of the segregation of the time scales. In fact, the videotape easily shows how the motion of the vortices is quite regular, at least during the last phases of the dynamic evolution; in any case, it involves time scales much larger than any other time scales. Vortex circulation time, for example, can be very well appreciated from the videotape, especially during the many merging events.

Conversely, in the field of three-dimensional flows, mathematical analysis has never been able to provide any synthetic description of the behavior of the system, except for some limited results; a graphical representation of the three-dimensional fields still appears to be the only useful tool. Now time-dependent animations, such as the ones presented here for different observation directions, appear to cast more light on the dynamic evolution and, while confirming some of the previously published results ([36]), will probably become a standard in the near future.

[7] graPHIGS is a trademark of International Business Machines Corporation.

Acknowledgments

The authors wish to thank George F. Carnevale for his help during his stay as a visiting scientist at ECSEC; they are also indebted to A. De Castro, F. Grassani, M. Marrone, F. Pedullá, F. Schiattarella, and T. Tonelli for their collaboration in producing the visualization of the numerical experiments.

References

1. L. D. Landau and E. M. Lifschitz, *Mécanique des Fluides*, M.I.R., Moscow, 1971.
2. G. K. Batchelor, *An Introduction to Fluid Dynamics*, Cambridge University Press, Cambridge, England, 1967.
3. A. S. Monin and A. M. Yaglom, *Statistical Fluid Mechanics*, Vol. 1, MIT Press, Cambridge, MA, 1975.
4. A. N. Kolmogorov, "The Local Structure of Turbulence in Incompressible Viscous Fluid for Very Large Reynolds Numbers," *C.R. Acad. Sci. URSS* **30,** 301 (1941).
5. R. Benzi, G. Paladin, G. Parisi, and A. Vulpiani, "On the Multifractal Nature of Fully Developed Turbulence and Chaotic Systems," *J. Phys. A: Math. Gen.* **17,** 3521 (1984).
6. F. Anselmet, Y. Cagne, E. J. Hopfinger, and R. A. Antonia, "High-Order Velocity Structure Functions in Turbulent Shear Flows," *J. Fluid Mech.* **140,** 63 (1984).
7. M. Ottaviani, F. Romanelli, R. Benzi, M. Briscolini, P. Santangelo, and S. Succi, "Numerical Studies of Ion Temperature Gradient Driven Turbulence," *Phys. Fluids B* **2,** 67 (1990).
8. C. Basdevant, B. Legras, R. Sadourny, and M. Beland, "A Study of Barotropic Model Flows: Intermittency Waves and Predictability," *J. Atmos. Sci.* **38,** 2305 (1981).
9. J. C. McWilliams, "The Emergence of Isolated Coherent Vortices in Turbulent Flow," *J. Fluid Mech.* **146,** 21 (1984).
10. P. Santangelo, R. Benzi, and B. Legras, "The Generation of Vortices in High-Resolution, Two-Dimensional Decaying Turbulence and the Influence of Initial Conditions on the Breaking of Self-Similarity," *Phys. Fluids A* **1,** 1027 (1989).
11. B. Legras, P. Santangelo, and R. Benzi, "High-Resolution Numerical Experiments for Forced Two-Dimensional Turbulence," *Europhys. Lett.* **5,** 37 (1988).
12. R. H. Kraichnan, "Inertial Ranges of Two-Dimensional Turbulence," *Phys. Fluids* **10,** 1417 (1967).
13. G. K. Batchelor, "Computation of the Energy Spectrum in Homogeneous Two-Dimensional Turbulence," *Phys. Fluids Suppl.* 2 **12,** 233 (1969).
14. A. Babiano, C. Basdevant, B. Legras, and R. Sadourny, "Dynamique Comparées du Turbillon et d'un Scalaire Passif en Turbulence Bi-Dimensionelle," *C. R. Acad. Sci. Paris* **299,** Series 2, 601 (1984).
15. R. Benzi, S. Patarnello, and P. Santangelo, "Self-Similar Coherent Structures in Two-Dimensional Decaying Turbulence," *J. Phys. A: Math. Gen.* **21,** 1221 (1988).
16. S. A. Orszag, "Numerical Simulations of Incompressible Flows Within Simple Boundaries. I. Galerkin (Spectral) Representations," *Stud. Appl. Math.* **50,** 293 (1971).
17. G. S. Patterson, Jr. and S. A. Orszag, "Spectral Calculations of Isotropic Turbulence: Efficient Removal of Aliasing Interactions," *Phys. Fluids* **14,** 2538 (1971).

18. *IBM ESSL, Engineering and Scientific Subroutine Library, Guide and Reference, Release 3*, Order No. SC23-0184-3, 1988; available through IBM branch offices.
19. *IBM VS FORTRAN, Version 2, Programming Guide, Release 3*, Order No. SC26-4222-3, 1988; available through IBM branch offices.
20. *IBM Parallel FORTRAN, Version 2, Language and Library Reference*, Order No. SC23-0431-0, 1988; available through IBM branch offices.
21. R. Benzi, S. Patarnello, and P. Santangelo, "On the Statistical Properties of Two-Dimensional Decaying Turbulence," *Europhys. Lett.* **3,** 811 (1987).
22. M. V. Melander, N. J. Zabusky, and J. C. McWilliams, "Symmetric Vortex Merger in Two Dimensions: Causes and Conditions," *J. Fluid Mech.* **195,** 303 (1988).
23. J. C. McWilliams, "Interaction of Isolated Vortices," *Geophys. Astrophys. Fluid. Dynam.* **24,** 1 (1983).
24. A. Babiano, C. Basdevant, B. Legras, and R. Sadourny, "Vorticity and Passive-Scalar Dynamics in Two-Dimensional Turbulence," *J. Fluid Mech.* **183,** 379 (1987).
25. M. E. Brachet, M. Meneguzzi, and P. L. Sulem, "Small-Scale Dynamics of the High Reynolds Number Two-Dimensional Turbulence," *Phys. Rev. Lett.* **57,** 683 (1986).
26. M. E. Brachet, M. Meneguzzi, H. Politano, and P. L. Sulem, "The Dynamics of Freely Decaying Two-Dimensional Turbulence," *J. Fluid Mech.* **194,** 333 (1988).
27. S. Kida, "Numerical Simulation of Two-Dimensional Turbulence with High Symmetry," *J. Phys. Soc. Jpn.* **54,** 2840 (1985).
28. Ye. A. Novikov, "Spectral Inequalities for Two-Dimensional Turbulence," *Izv. Atm. Ocean. Phys.* **14,** 474 (1978).
29. M. Lesieur and R. Rogallo, "Large-Eddy Simulations of Passive Scalar Diffusion in Isotropic Turbulence," *Phys. Fluids A* **1,** 718 (1989).
30. R. S. Rogallo and P. Moin, "Numerical Simulations of Turbulent Flows," *Ann. Rev. Fluid Mech.* **16,** 99 (1984).
31. V. Yakhot and S. A. Orszag, "Renormalization Group Analysis of Turbulence. I. Basic Theory," *J. Sci. Comp.* **1,** 1 (1986).
32. R. H. Kraichnan, "An Interpretation of the Yakhot–Orszag Turbulence Theory," *Phys. Fluids* **30,** 2400 (1987).
33. F. Hussain, "Coherent Structures and Turbulence," *J. Fluid Mech.* **173,** 303 (1986).
34. M. M. Rogers and P. Moin, "Helicity Fluctuations in Incompressible Turbulent Flows," *Phys. Fluids* **30,** 2662 (1987).
35. E. Levich and E. Tzvetkov, "Certain Problems in the Theory of Developed Hydrodynamical Turbulence," *Phys. Rep.* **128,** 1 (1987).
36. M. V. Melander and N. J. Zabusky, "Interaction and 'Apparent' Reconnection of 3D Vortex Tubes via Direct Numerical Simulations," *Fluid Dynam. Res.* **3,** 247–250 (1988).
37. M. V. Melander and F. Hussain, "Cross-Linking of Two Antiparallel Vortex Tubes," *Phys. Fluids A* **1,** 633 (1989).
38. N. J. Zabusky and M. V. Melander, "Three Dimensional Vortex Tube Reconnection: Morphology for Orthogonally-Offset Tubes," *Physica D* **37,** 555 (1989).
39. P. Moin, A. Leonard, and J. Kim, "Evolution of a Curved Vortex Filament into a Vortex Ring," *Phys. Fluids* **29,** 955 (1986).
40. *IBM Image Access Executive, IAX, Program Description and Operations Manual, Release 1.0*, Order No. SB11-8415-0, 1988; available through IBM branch offices.
41. *Int. J. Supercomput. Appl.* **4,** No. 2 (1990).
42. M. Briscolini and P. Santangelo, "A Multi User Recording System for Video Animation," *IBM ECSEC Technical Report*, in preparation, 1991.
43. M. Bernaschi, E. Marinari, S. Patarnello, and S. Succi, "Three-Dimensional Visualization of Many-Body System Dynamics," *IBM J. Res. Develop.* **35,** 254–269 (1991, this issue).
44. W. E. Lorensen and H. E. Cline, "Marching Cubes: A High Resolution 3D Surface Construction Algorithm," *Comput. Graph.* **21,** 163 (1987).
45. *The graPHIGS Programming Interface, Subroutine Reference, Version 2, Release 1*, Order No. SC33-8194-0, 1989; available through IBM branch offices.
46. *The graPHIGS Programming Interface, Understanding Concepts, Version 2, Release 1*, Order No. SC33-8191-0, 1989; available through IBM branch offices.

Received November 20, 1989; accepted for publication August 14, 1990

Tape caption

The tape contains the video animation of the two high-resolution (512 × 512) numerical experiments of decaying turbulence described in Section 2. The first one starts from a Kraichnan–Batchelor spectrum [$E(k) \sim k^{-3}$, Figure 1]; the second one starts from a steep spectrum [$E(k) \sim k^{-6}$, Figure 11]. In both cases we show the evolution of the vorticity field for 40 time units; the colors are the same for Figures 1 and 11. Successively, we present animations of the dynamic evolutions of two initially orthogonally offset vorticity tubes with numerical spatial resolution 128 × 128 × 128 as described in Section 3. An isovorticity surface representation is used to show the evolution. The first three pieces show the same system, namely case 1, composed by two initially approximately equal vorticity tubes, as seen from three different observation directions; the isovorticity value and the Euler angles are as in Figure 16. The second three pieces show the dynamic evolution of case 2; here, the secondary vortex is initially much fainter than the primary one. The dynamic evolution makes the secondary vortex tube visible above the chosen vorticity threshold as a consequence of its continuous stretching, resulting from circular dragging around the main tube. The isovorticity value and the Euler angles are as in Figure 20.

Marco Briscolini *IBM European Center for Scientific and Engineering Computing (ECSEC), Via Giorgione 159, 00147 Rome, Italy.* Dr. Briscolini received his doctorate in physics in 1984 and his Ph.D. in aerospace engineering in 1989 from the University of Rome. He joined IBM in 1987 and since that time has worked on computational fluid dynamics, focusing his attention on high-resolution numerical simulations of two-dimensional and three-dimensional turbulent flows. Concurrently, he has been active on the project of scientific visualization at ECSEC. He has also contributed to the porting of industrial codes for crash analysis on the IBM 3090 Vector Multiprocessor.

Paolo Santangelo *IBM European Center for Scientific and Engineering Computing (ECSEC), Via Giorgione 159, 00147 Rome, Italy.* Dr. Santangelo received his doctorate in physics from Rome University in 1979. From 1980 to 1983 he was a researcher at the Astronomical Institute of Rome University, where he worked on the dynamical evolution of groups and clusters of galaxies. In 1984, he joined IBM Rome Scientific Center, where he worked in the field of mathematical modeling of hydrological systems. Dr. Santangelo is now a permanent research staff member of the IBM European Center for Scientific and Engineering Computing (ECSEC), where he has worked on high-resolution numerical computations for two-dimensional turbulence and three-dimensional flows. In 1986 Dr. Santangelo received an IBM Outstanding Technical Achievement Award for his work on the parallel implementation of the gravitational N-body problem on the ECSEC Loosely Coupled Parallel System. Subsequently he worked on the porting of industrial codes for the simulation of oil reservoirs on the IBM 3090 Vector Facility and in 1989 received an IBM Outstanding Technical Achievement Award for his contribution to that project. Dr. Santangelo has published numerous papers in the field of astrophysics and fluid dynamics. His current interests are in scientific visualization.